Supplemental Information: Significant phase deviation of magnetic quantum oscillations induced by magnetic impurities

Sang-Eon Lee[1,2], Sanghyun Ji[1,3], Myung-Hwa Jung[1,*]

[1]*Department of Physics, Sogang University, Seoul 04107, Republic of Korea,*

[2]*National High Magnetic Field Laboratory, Tallahassee, Florida 32310, USA,*

[3]*Department of Materials Science and Engineering, Yonsei University, Seoul 03722, Republic of Korea*

Supplemental Information includes:

*Contact authors: mhjung@sogang.ac.kr

Note 1. Semiclassical two-carrier model fitting

The MR and Hall resistivities were analyzed using the semiclassical two-carrier model[1]:

$$\rho_{xx}(B) = \frac{1}{e}\frac{(n_h\mu_h + n_e\mu_e) + (n_h\mu_h + n_e\mu_e)\mu_h\mu_e B^2}{(n_h\mu_h + n_e\mu_e)^2 + (n_h - n_e)^2\mu_h^2\mu_e^2 B^2}, \quad \text{(S1)}$$

$$\rho_{yx}(B) = \frac{B}{e}\frac{(n_h\mu_h^2 - n_e\mu_e^2) + (n_h - n_e)^2\mu_h^2\mu_e^2 B^2}{(n_h\mu_h + n_e\mu_e)^2 + (n_h - n_e)^2\mu_h^2\mu_e^2 B^2}, \quad \text{(S2)}$$

where e is the elementary charge, $n_{e(h)}$ is electron (hole) carrier density, and $\mu_{e(h)}$ is the electron (hole) mobility. We simultaneously fitted the MR and Hall resistivity with Eq. (S1 and S2), respectively, with a constraint of $1/(en_e\mu_e + en_h\mu_h) = \rho_{xx}$ (B = 0 T). Figure S1(a-f and g-l) shows the MR and Hall resistivities and the fitted curves with Eq. (S1 and S2), respectively. The fitting parameters are listed in Table S1. Overall, the fitted curves are well-matched with the data, suggesting the dominant contribution of the semiclassical signals on the field dependence of ρ_{xx} and ρ_{yx}. While the semiclassical analysis provides a good estimation for the carrier densities and mobilities, other effects beyond the semiclassical framework, such as quantum interference effects [2–5] or guiding center diffusion[6,7] cannot be captured by the analysis. For Fe-doped samples, the Kondo effect[8] and anomalous Hall effect[9] should also be considered. These effects might be subtly imposed on the dominating semiclassical signals and would produce some errors in the fitting parameters.

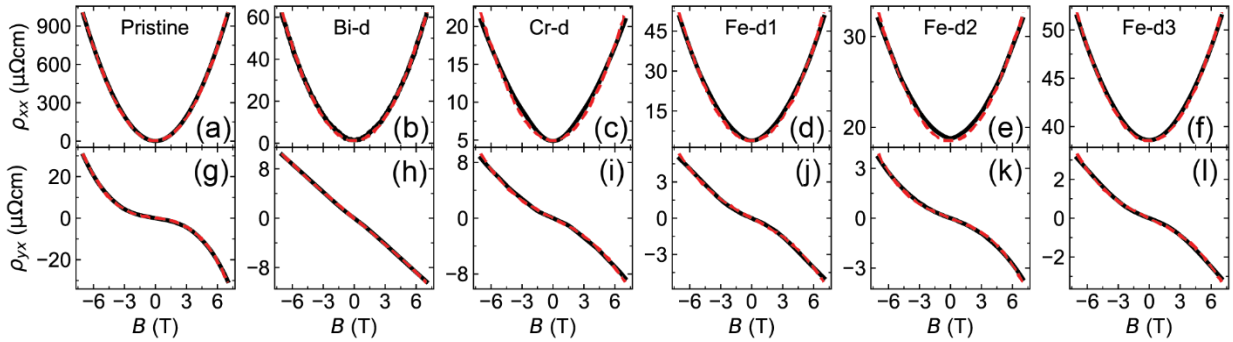

Fig. S1. Semiclassical two-carrier model fitting for the MR and Hall resistivities of Pristine, Bi-d, Cr-d, Fe-d1, Fe-d2, and Fe-d3 at 2 K. The black solid lines and red dashed lines represent the data and fitted curves, respectively. **a-f** Field-dependent ρ_{xx} and fitted curves with Eq. (S1). **g-l** Field-dependent ρ_{yx} and fitted curves with Eq. (S2).

Table S1. Fitting parameters obtained from the two-carrier model described by Eq. (S1 and S2).

	n_e ($\times 10^{20}$ cm^{-3})	n_h ($\times 10^{20}$ cm^{-3})	μ_e (m^2/Vs)	μ_h (m^2/Vs)	n_e/n_h	μ_e/μ_h
Pristine	2.369(7)	2.368(7)	21.6(1)	12.2(1)	1.0004	1.77
Bi-d	2.349(2)	2.341(1)	1.945(3)	0.619(1)	1.0034	3.142
Cr-d	2.413(2)	1.877(2)	0.3456(7)	0.2270(4)	1.2856	1.522
Fe-d1	1.634(6)	1.5941(4)	0.578(1)	0.4606(6)	1.0250	1.255
Fe-d2	1.572(2)	1.090(2)	0.1221(5)	0.1333(2)	1.4422	0.915
Fe-d3	1.148(1)	0.774(1)	0.0802(1)	0.0905(1)	1.4832	0.886

Note 2. Magnetic field correction procedure

In the system with a superconducting magnet, the sample magnetization or the superconducting magnetic fluxes[10] can give a magnetic field error in the reported magnetic field value from the actual magnetic field value, since the reported magnetic field value is calibrated from the measured electric current flowing through the superconducting magnet. These give an additional magnetic field ΔB added to the reported magnetic field, B_r, resulting in the actual magnetic field, $B_a = B_r + \Delta B$.

We first investigated the effect of the sample magnetization. Pristine, Bi-d, Cr-d, and Fe-d show the linear magnetic susceptibilities around $\chi \approx -1\times10^{-4}$ μ_B/f.u. T^{-1}. In this case, the additional magnetic field can be simply given by $\Delta B = \mu_0 a \chi B_r$, where a is the sample shape constant ranging from 0 to 1. The dHvA effects can be expressed as $\Delta M \sim \sin(2\pi F/B_a) = \sin[2\pi F/(B_r + \mu_0 a \chi B_r)] = \sin(2\pi F^*/B_r)$, where $F^* = F/(1 + \mu_0 a \chi)$. In this formalism, the report frequencies F^* are larger than F by an amount of $\approx$ 0.0017% for Pristine, Bi-d, Cr-d, and Fe-d.

The other effect of sample magnetization is the magnetic interaction[11], which is the effect of oscillatory magnetic field error caused by the dHvA effects. The magnetic interaction is only effective when the oscillatory magnetic field error is comparable to the peak-to-peak distance of the dHvA effect in the magnetic field domain. The maximum size of the oscillations for Pristine is around $\Delta M \approx 2\times10^{-4}$ μ_B/f.u. at 2 K, giving the oscillatory field error of $\approx$ 0.34 G, which is much smaller than the peak-to-peak distance of the dHvA effect in the magnetic field domain $\approx$ 70 G around B = 7 T. Therefore, we conclude that the magnetization interaction cannot produce significant errors in the dHvA analysis.

Second, we investigated the effect of the superconducting flux. The typical values of ΔB from the superconducting fluxes are shown in Fig S2a with different field sweep directions. We estimated ΔB of our superconducting magnet by subtracting the simulated Landau fan diagram satisfying $1/B = (N + 0.125)/F$ from the experimental Landau fan diagram of Pristine, assuming that the Landau fan diagram of Pristine is linear and has the x-intercept of $\gamma = -0.125$ without the magnetic field error. The value of F was appropriately chosen to reproduce the reasonable behavior and sizes of ΔB based on Fig S2a. Figure S2b shows the estimated ΔB for our superconducting magnet. We corrected magnetic fields with $B_a = B_r + \Delta B$ for the dHvA analysis using the estimated ΔB.

The phase analysis was much improved by the magnetic field correction. Figure S2(c-d) shows

the Landa fan diagram before and after correction, respectively. After correction, the values of intercept, γ, of Pristine, Bi-d, and Cr-d are much closer to the expected value of $\gamma = -0.125$. Overall, the phases are increased by 0.05-0.07, and the frequencies are decreased by 0.3-0.45. The value comparison is shown in Table S2.

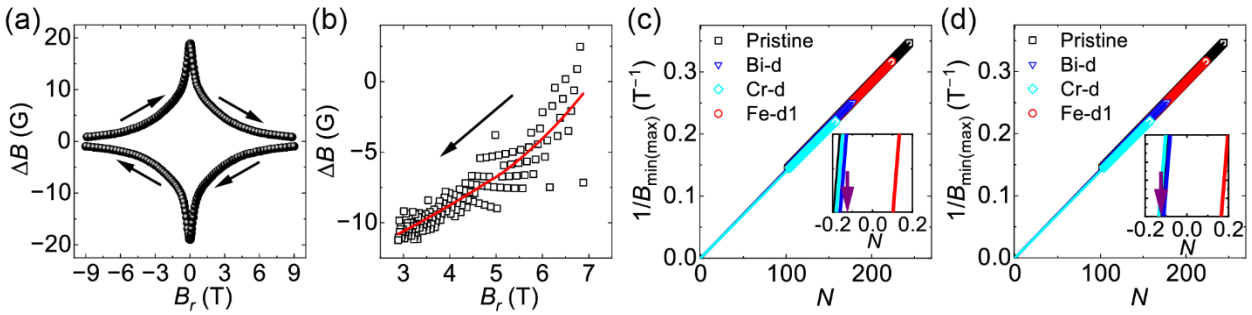

Fig. S2. Magnetic field error of the superconducting magnet and comparison of the Landau fan diagram before and after magnetic field correction. a Typical magnetic field error from the superconducting fluxes. The arrows display the field sweep directions. The data was borrowed from the application note of Quantum Design [10]. **b** Magnetic field error of our superconducting magnet estimated by subtracting the simulated Landau fan diagram satisfying $1/B = (N + 0.125)/F$ from the experimental Landau fan diagram of Pristine. The arrow indicates the field sweep direction. The red line is the smooth curve capturing the trend, which is used for magnetic field error correction. **c-d** Landan fan diagrams of Pristine, Bi-d, Cr-d, and Fe-d before and after magnetic field correction, respectively. The insets are the magnified views of the intercepts. The purple arrows indicate $N = -0.125$.

Table S2. Comparison between the frequencies and phases of dHvA effects before and after magnetic field correction. The subscripts *bc* and *fc* denote "before correction" and "after correction".

F_{bc} (T)	F_{fc} (T)	γ_{bc}	γ_{fc}	ΔF	$\Delta\gamma$
704.660(5)	704.218(3)	−0.192(1)	−0.123(1)	−0.442	0.069
708.93(1)	708.58(1)	−0.162(3)	−0.111(3)	−0.35	0.051
717.4(1)	717.1(1)	−0.18(2)	−0.13(2)	−0.3	0.05
705.36(1)	704.94(1)	0.103(3)	0.165(3)	−0.42	0.062

References

1. Ashcroft, N. W. & Mermin, N. D. *Solid State Physics*. (Saunders College Publishing, 1976).

2. Salawu, Y. A., Yun, J. H., Rhyee, J.-S., Sasaki, M. & Kim, H.-J. Weak antilocalization, spin–orbit interaction, and phase coherence length of a Dirac semimetal $Bi_{0.97}Sb_{0.03}$. *Sci. Rep.* **12,** 2845 (2022).

3. Nakamura, H., Huang, D., Merz, J., Khalaf, E., Ostrovsky, P., Yaresko, A., Samal, D. & Takagi, H. Robust weak antilocalization due to spin-orbital entanglement in Dirac material Sr_3SnO. *Nat. Commun.* **11,** 1161 (2020).

4. Fu, B., Wang, H. W. & Shen, S. Q. Quantum Interference Theory of Magnetoresistance in Dirac Materials. *Phys. Rev. Lett.* **122,** 246601 (2019).

5. Chen, W., Lu, H. Z. & Zilberberg, O. Weak localization and antilocalization in nodal-line semimetals: Dimensionality and topological effects. *Phys. Rev. Lett.* **122,** 196603 (2019).

6. Song, J. C. W., Refael, G. & Lee, P. A. Linear magnetoresistance in metals: Guiding center diffusion in a smooth random potential. *Phys. Rev. B* **92,** 180204 (2015).

7. Leahy, I. A., Lin, Y. P., Siegfried, P. E., Treglia, A. C., Song, J. C. W., Nandkishore, R. M. & Lee, M. Nonsaturating large magnetoresistance in semimetals. *Proc. Natl. Acad. Sci. U.S.A.* **115,** 10570–10575 (2018).

8. Costi, T. A. Kondo Effect in a Magnetic Field and the Magnetoresistivity of Kondo Alloys. *Phys. Rev. Lett.* **85,** 1504–1507 (2000).

9. Nagaosa, N., Sinova, J., Onoda, S., MacDonald, A. H. & Ong, N. P. Anomalous Hall effect. *Rev. Mod. Phys.* **82,** 1539–1592 (2010).

10. Quantum Design. *Application Note 1070-207: Using PPMS Superconducting Magnets at Low Fields*. (2009).

11. D. Shoenberg & F. R. S. *Magnetic oscillations in metals*. (Cambridge University Press, 1984).